

# Crystal Structure of Rhodopsin: A G Protein–Coupled Receptor

Krzysztof Palczewski,<sup>1,2,3\*</sup> Takashi Kumasaka,<sup>7</sup> Tetsuya Hori,<sup>7,8</sup>  
 Craig A. Behnke,<sup>4,6</sup> Hiroyuki Motoshima,<sup>7</sup> Brian A. Fox,<sup>4,6</sup>  
 Isolde Le Trong,<sup>5,6</sup> David C. Teller,<sup>4,6</sup> Tetsuji Okada,<sup>1</sup>  
 Ronald E. Stenkamp,<sup>5,6\*</sup> Masaki Yamamoto,<sup>7</sup> Masashi Miyano<sup>7\*</sup>

Heterotrimeric guanine nucleotide-binding protein (G protein)–coupled receptors (GPCRs) respond to a variety of different external stimuli and activate G proteins. GPCRs share many structural features, including a bundle of seven transmembrane  $\alpha$  helices connected by six loops of varying lengths. We determined the structure of rhodopsin from diffraction data extending to 2.8 angstroms resolution. The highly organized structure in the extracellular region, including a conserved disulfide bridge, forms a basis for the arrangement of the seven-helix transmembrane motif. The ground-state chromophore, 11-*cis*-retinal, holds the transmembrane region of the protein in the inactive conformation. Interactions of the chromophore with a cluster of key residues determine the wavelength of the maximum absorption. Changes in these interactions among rhodopsins facilitate color discrimination. Identification of a set of residues that mediate interactions between the transmembrane helices and the cytoplasmic surface, where G-protein activation occurs, also suggests a possible structural change upon photoactivation.

GPCRs activate signaling paths in response to stimuli such as  $\text{Ca}^{2+}$ , amines, hormones, peptides, and even large proteins (1–3). GPCRs share a conserved transmembrane structure comprising seven  $\alpha$  helices. Binding of specific ligands to the extracellular or transmembrane domains causes conformational changes that act as a switch to relay the signal to G proteins that in turn evoke further intracellular responses (4).

Rhodopsins are a member of the largest subfamily, constituting ~90% of all GPCRs. These are activated by light and turn on the signaling pathway that leads to vision. Mutations in the rhodopsin gene lead to human retinal pathologies (5). Rhodopsin is composed of the protein opsin (~40 kD in size) covalently linked to 11-*cis*-retinal (a derivative of vitamin A) through Lys<sup>296</sup> (6, 7). Absorption of a photon by the 11-*cis*-retinal causes its isomerization to all-*trans*-retinal (8), leading to a conformational change of the protein moiety, including the cytoplasmic surface. The photolyzed chromophore only

transiently activates opsin, before the all-*trans*-retinal is hydrolyzed and dissociated from the opsin. Rhodopsin is regenerated by newly synthesized 11-*cis*-retinal delivered from adjacent retinal epithelial cells. The absorption of a single photon results in the activation of hundreds of G-protein molecules with extraordinary reproducibility (9), whereas the 11-*cis*-retinal-bound rhodopsin has extremely low activity. These two properties allow the human scotopic visual system to detect as few as five photons (10).

A low-resolution structure of frog rhodopsin that reveals the organization of the seven transmembrane helices has been determined by cryo-electron microscopy (11), and biochemical and theoretical studies have given further insights into rhodopsin structure and function (12–18). Here, we describe the three-dimensional (3D) crystal structure of rhodopsin at 2.8 Å. This gives further insights into the mechanisms of receptor activation, and the source of specific ligand and G-protein interactions.

**Structure determination: Overall fold and molecular contacts.** To obtain structural information for rhodopsin in the ground state, diffraction data for bovine rhodopsin crystallized from mixed micelles (19) were collected to 2.8 Å after mercury soaking. Phasing information was obtained employing multi-wavelength anomalous diffraction (MAD) methods (20). The least twinned data were selected after the collection of several MAD data sets. Initial calculations were performed without correction for twinning for 3.3 Å data set. The majority of other crystals examined were nonisomorphous and highly merohedrally twinned (20).

Rhodopsin molecules are packed in the crystal lattice to form an array of helical tubes (Fig. 1). The two molecules in the asymmetric unit are related by a noncrystallographic twofold axis between the two H-I helices. The current model of bovine rhodopsin (Fig. 2) includes all 194 residues that make up seven transmembrane helices; these are 35 to 64 for H-I, 71 to 100 for H-II, 107 to 139 for H-III, 151 to 173 for H-IV, 200 to 225 for H-V, 247 to 277 for H-VI, and 286 to 306 for H-VII (Fig. 2, A through C), 74 of 348

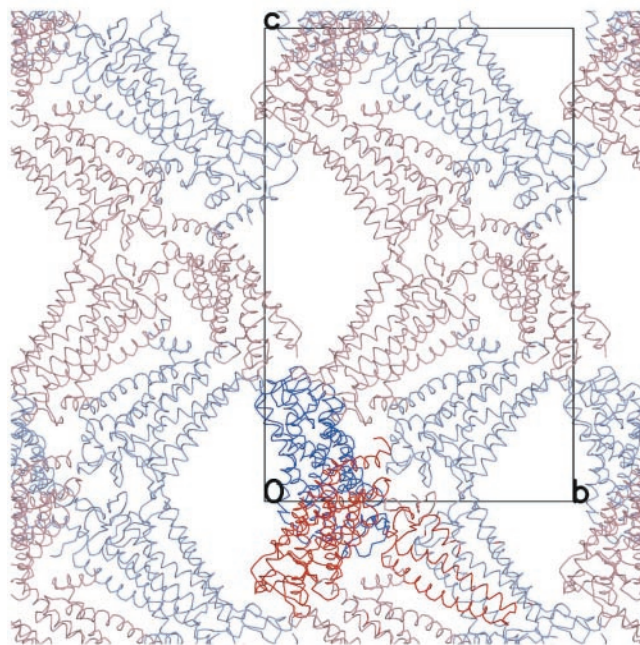


**Fig. 1.** Molecular packing viewed along the **a** axis of the crystal. A unit cell is superposed. One of the asymmetric units containing two rhodopsin molecules is drawn with thick lines. The NCS axis is nearly parallel to the crystallographic **a** axis.

<sup>1</sup>Department of Ophthalmology, <sup>2</sup>Department of Pharmacology, <sup>3</sup>Department of Chemistry, <sup>4</sup>Department of Biochemistry, <sup>5</sup>Department of Biological Structure, and <sup>6</sup>Biomolecular Structure Center, University of Washington, Seattle, WA 98195, USA. <sup>7</sup>Structural Biophysics Laboratory, RIKEN Harima Institute, 1-1-1 Kouto, Mikazuki-cho, Sayo-gun, Hyogo 679-5148, Japan. <sup>8</sup>Graduate School of Bioscience and Biotechnology, Tokyo Institute of Technology, 4259 Nagatsuta, Midori-ku, Yokohama 226-8501, Japan

\*To whom correspondence should be addressed. E-mail: miyano@spring8.or.jp (M.M.); palczews@u.washington.edu (K.P.); stenkamp@u.washington.edu (R.E.S.).

residues from the extracellular region; 1 to 34 for NH<sub>2</sub>-terminal tail, 101 to 106 for E-I, 174 to 199 for E-II, and 278 to 285 for E-III; 70 residues in the cytoplasmic region; and 65 to 70 for C-I, 140 to 150 for C-II, 226 to 235 and 240 to 246 for C-III, and 307 to 327 and 334 to 348 for the COOH-terminal region. Thus, a total of 338 amino acids in our model correspond to 97.1% of the whole opsin molecule, although the last 15-amino acid COOH-terminal segment is modeled as Ala residues. In addition, the 11-*cis*-retinal chromophore connected to Lys<sup>296</sup>, a part of two oligosaccharides at Asn<sup>2</sup>, Asn<sup>15</sup> (21), two Zn ions, three Hg ions, and some water molecules are also included per monomer in the current structural model.

**Comparison to other receptors.** Our current experimental model of rhodopsin offers a structural template for other GPCRs,

including the assignment of secondary structural elements and the location of highly conserved amino acids. The molecular size of bovine rhodopsin, 348 amino acids, is intermediate among the members of the family and thus can feature most of the essential parts of functional importance in G-protein activation. The lengths of the seven transmembrane helices and of the three extracellular loops are expected to be nearly the same for most of the family members, as can be seen in the sequence of  $\beta$ -adrenergic receptor (Web fig. 1) (22). Variation in other regions probably reflects the specificity of each receptor for either its ligand or its G protein. Because most of the vertebrate visual pigments share similar size distributions for all of the domains, structure-function relationships deduced from the current model are likely to be directly applicable to the mem-

bers of this subfamily. The structure of bovine rhodopsin, represented schematically in Fig. 3, contains many features found in most GPCRs, and clearly demonstrates many differences between GPCRs and bacterial retinal-binding proteins (23–25). Although the mass of transmembrane bundles of rhodopsin and bacterial rhodopsins does not differ significantly, the arrangements of seven helices are found to be different. The structure of rhodopsin disclosed larger and more organized extramembrane regions than that of bacteriorhodopsins, demonstrating the functional differences between these two retinal-binding proteins.

**Extracellular region.** Regions in the extracellular domain of rhodopsin (NH<sub>2</sub>-terminal and interhelical loops E-I, E-II, and E-III) associate to form a compact structure (Fig. 2 and Fig. 4A). The NH<sub>2</sub>-terminal tail of rhodopsin contains five distorted strands. The NH<sub>2</sub>-terminus is located just below loop E-III, with the side chain of Asp<sup>282</sup> close to that of Asn<sup>2</sup>. The first two antiparallel strands, Gly<sup>3</sup> to Pro<sup>12</sup>, form a typical  $\beta$ -sheet fold ( $\beta$ 1 and  $\beta$ 2) running almost parallel to the expected plane of the membrane. Strands three to five (S3-S5) form a right triangle from Phe<sup>13</sup> to Pro<sup>34</sup>, with the third strand running just below E-III, almost parallel to the long axis of the molecule. S4 connects Ser<sup>14</sup>-Asn<sup>15</sup> in the NH<sub>2</sub>-terminal region of the molecule with Pro<sup>23</sup>, located close to E-I. S5 from Pro<sup>27</sup> to Pro<sup>34</sup> runs along the surface of the membrane covering the extracellular (intradiscal) space between H-I and H-II. Oligosaccharides at Asn<sup>2</sup> and Asn<sup>15</sup> extend from the domain and are not included in any interactions. Mutations of Pro<sup>23</sup> or Gln<sup>28</sup> cause the eye disease retinitis pigmentosa (5). These side chains are located close together in a region between the S4 and S5 strands and are also close to the side chain of Tyr<sup>102</sup> from the E-I loop. Thus, these residues may maintain the proper orientation between E-I and the NH<sub>2</sub>-terminal domain. The NH<sub>2</sub>-terminal domain may also contact the E-III loop in the region of Pro<sup>12</sup>.

While both the E-I and E-III loops run along the periphery of the molecule, a part of E-II folds deeply into the center of rhodopsin. From the extracellular end of H-IV, a long strand from Gly<sup>174</sup> to Met<sup>183</sup> crosses the molecule along the membrane surface. The terminal two residues, Met<sup>183</sup> and Gln<sup>184</sup>, have extended side chains. The former points to a hydrophobic pocket around H-I while the latter is surrounded by hydrophilic groups, including a water molecule located close to peptide carbonyl of Pro<sup>180</sup> and OH group of Tyr<sup>192</sup>. Residues in the middle of this strand, Arg<sup>177</sup> to Glu<sup>181</sup> ( $\beta$ 3), form an antiparallel  $\beta$ -sheet with residues, Ser<sup>186</sup> to Asp<sup>190</sup> ( $\beta$ 4), which is deeper inside the molecule than  $\beta$ 3.  $\beta$ 4 is just below the 11-*cis*-retinal and is a part of the chromophore-binding pocket.

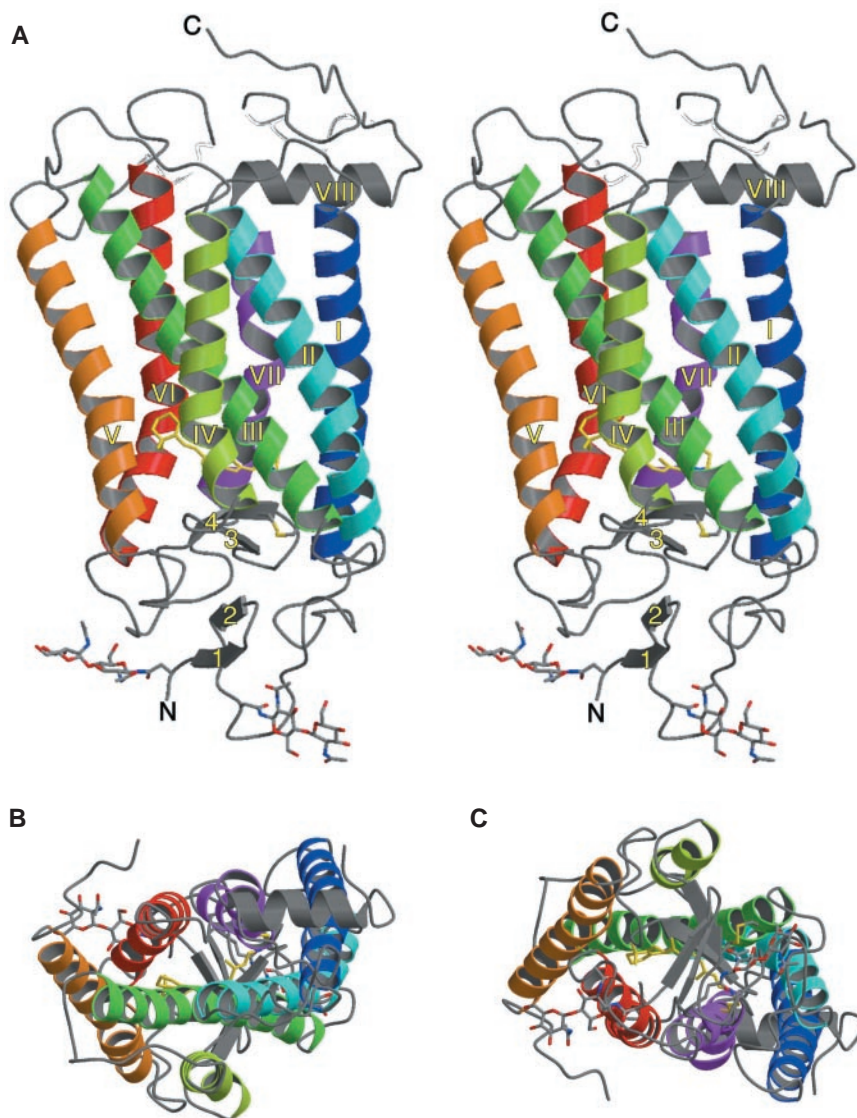


**Fig. 2.** Ribbon drawings of rhodopsin. (A) Parallel to the plane of the membrane (stereoview). A view into the membrane plane is seen from the cytoplasmic (B) and intradiscal side (C) of the membrane.



**Fig. 4.**  $C_{\alpha}$ -traces showing the packing of the polypeptide, with some key residues described in the text, on the (A) intradiscal side and (B) the cytoplasmic side of the molecule. Colors of the side chains are red for acidic, blue for basic, yellow for polar, and gray for nonpolar group.

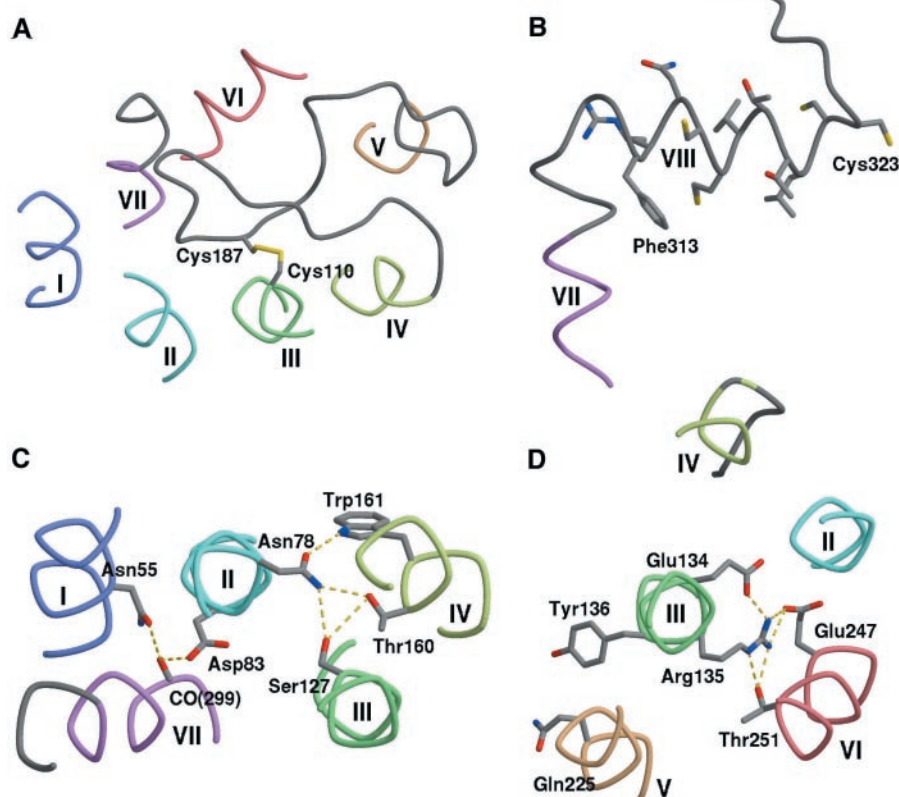
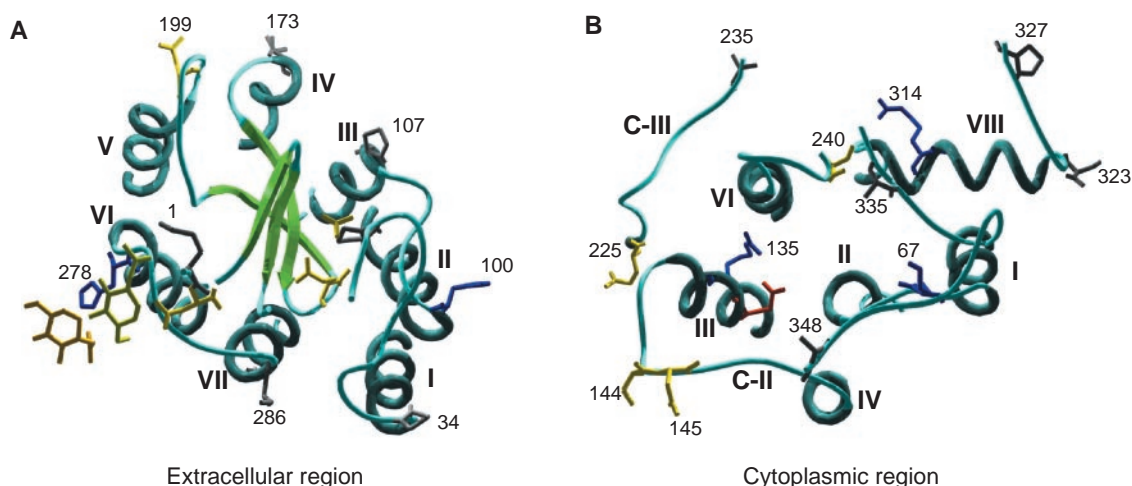


**Fig. 5.** Structural details for four regions in rhodopsin. (A) The E-II loop near the disulfide bridge connecting Cys<sup>110</sup> and Cys<sup>187</sup>, viewed from extracellular side. (B) The C-IV cytoplasmic loop from Lys<sup>311</sup> to Leu<sup>321</sup> forming a short amphiphilic helix (H-VIII). (C) Interhelical hydrogen bonds mediated by a highly conserved Asn<sup>55</sup>, connecting H-I, H-II, and H-VII, and by Asn<sup>78</sup> for H-II, H-III, and H-IV. (D) The tripeptide region, Glu<sup>134</sup>-Arg<sup>135</sup>-Tyr<sup>136</sup>, known as a (D/E)R(Y/W) motif located near the cytoplasmic end of H-III.

to be determined by a significant bend around Pro<sup>267</sup>. From H-IV, only Cys<sup>167</sup> participates covering a part of this pocket. Residues from H-I, H-II, and H-VII and Tyr<sup>43</sup>, Met<sup>44</sup>, Leu<sup>47</sup>, Thr<sup>94</sup>, and Phe<sup>293</sup> are part of the region surrounding the Schiff base. Finally, the extracellular side of the polyene chain is covered by a part of the E-II loop,  $\beta$ -sheet  $\beta 4$  from Ser<sup>186</sup> to Ile<sup>189</sup>. The side chain of Glu<sup>181</sup> in

$\beta 3$  of the E-II loop points toward the retinylidene group, supporting the previous results demonstrating that the corresponding amino acid in red/green pigments may be the binding site for chloride ion, which is responsible for the red shift in their absorption compared with rhodopsin (37). Another amino acid from the E-II loop participating in the retinylidene group binding site is Tyr<sup>191</sup>, whose

OH group is also close to that of Tyr<sup>268</sup> in H-VI. Since mutation of this residue does not affect the absorption but reduces the ability to activate transducin (38), it may participate in the transition to the active form of rhodopsin through interaction with Tyr<sup>268</sup>.

The arrangement around the Schiff base is of particular interest in terms of understanding the mechanism of the primary process in photoactivation of rhodopsin. The direction of the side chain of Lys<sup>296</sup>, almost along the long axis of rhodopsin, is supported by two hydrophobic side chains in H-I, Met<sup>44</sup> and Leu<sup>47</sup>, and by a nearby peptide bond between Phe<sup>293</sup> and Phe<sup>294</sup>. This region is stabilized through the two phenyl rings interacting with other helices. Since it is difficult to determine exactly from the current structure how the protonated Schiff base linkage is stabilized in the protein environment, our model cannot discriminate whether any water molecules participate in making a complex counterion (39) or not. The distances between the carboxylate oxygen atoms of Glu<sup>113</sup> and the Schiff base nitrogen are 3.3 Å and 3.5 Å. Also, the OH group of Thr<sup>94</sup> comes close to one of the oxygen atoms of Glu<sup>113</sup> with a distance of 3.4 Å. Any other residues, including the nearby Thr<sup>92</sup> and Thr<sup>93</sup>, are too far from the Schiff base region to contribute to stabilization of its protonated state. Further improvements in resolution will provide more detailed views of this region.

**Cytoplasmic surface.** The structure around the C-I loop exhibits a rigid organization (Fig. 4B). Of the three basic side chains in this region, Lys<sup>67</sup> projects toward the solvent, whereas Lys<sup>66</sup> and Arg<sup>69</sup> point toward lipid-facing region. Another basic side chain of His<sup>65</sup> sits closely to C-IV loop (H-VIII). The side chain of Lys<sup>67</sup> appears to interact with a part of COOH-terminal tail region, which runs nearly parallel to C-I. The extreme COOH-terminal residues are the most exposed part of rhodopsin molecule and could be involved in vectorial transport of

**Table 1.** Statistics for data collection, phasing, and refinement.

Data collection and phasing							
Space group	P4 <sub>1</sub>						
Beamline	SPring-8 BL45XU						APS 19-ID
Unit cell	a = 96.73, c = 149.63 Å						a = 97.25, c = 149.54 Å
Resolution (Å)	3.3 (MAD)						2.8 (Refine)
Data set	Remote 1	Edge 1	Peak 1	Remote 2	Edge 2	Peak 2	High resolution
Wavelength (Å)	0.96000	1.00876	1.00800	1.04000	1.00866	1.00700	1.000
Observed reflections	66,421	66,589	66,651	75,521	74,715	73,063	111,245
Unique reflections	20,499	20,529	20,541	20,636	20,613	20,624	33,221
Completeness*	99.0 (99.5)	99.2 (99.7)	99.1 (99.4)	99.4 (99.8)	99.3 (99.7)	99.3 (99.8)	97.1 (80.7)
I/σ	12.6 (3.6)	11.9 (3.3)	10.6 (2.6)	11.1 (2.4)	11.7 (3.6)	11.6 (3.2)	7.8 (1.2)
R <sub>merge</sub> *†	8.5 (39.3)	9.2 (43.6)	10.0 (55.3)	10.6 (54.6)	10.3 (51.3)	10.4 (53.5)	12.1 (69.3)
Phasing power‡	0.0/1.1/–	0.6/1.0/0.4	0.9/1.0/0.7	1.6/1.0/1.1	1.5/1.1/1.1	1.4/1.2/1.0	
Figure of merit	0.37/0.31						
Twin fraction							0.288
Refinement statistics				Model statistics			
Resolution range (Å)	30.0–2.8			R <sub>msd</sub> from ideality			
R <sub>cryst</sub> § (%) (all data)	19.28			Bond length (Å)	0.0101		
R <sub>free</sub> (%) (all data)	23.97			Bond angle (degree)	1.41		
Reflections (completeness)				Ramachandran plot			
Working set	30,094 (88.0%)			Favored (%)	80.8		
Test set	1,525 (4.5%)			Allowed (%)	17.2		
Number of atoms	5,275			Generously allowed (%)	1.8		
Average B values (Å <sup>2</sup> )	53.9			Disallowed (%)	0.2		
Retinal (A/B) only (Å <sup>2</sup> )	27.53/32.01						

\*Values in parentheses indicate the highest resolution shell. † $R_{\text{merge}} = \sum_{\text{hkl}} \sum_i |I_i(\text{hkl}) - \langle I(\text{hkl}) \rangle| / \sum_{\text{hkl}} \sum_i I_i(\text{hkl})$ . ‡Phasing power =  $F_{\text{H(calc)}}/E$ , where E is phase-integrated lack-of-closure. The three values for each wavelength are for acentric isomorphous/acentric anomalous/centric contribution. § $R_{\text{cryst}} = \sum_{\text{hkl}} |F_{\text{obs}}(\text{hkl}) - F_{\text{calc}}(\text{hkl})| / \sum_{\text{hkl}} F_{\text{obs}}(\text{hkl})$ . ||Values calculated except glycines and prolines.

rhodopsin to rod outer segment.

We assign the region from Cys<sup>140</sup> to Glu<sup>150</sup> as the C-II loop. This loop exhibits an L-shaped structure, when viewed parallel to membrane plane, with a barrel (Met<sup>143</sup> to Phe<sup>146</sup>) almost along the main axis of rhodopsin. Four polar side chains in this loop (Lys<sup>141</sup>, Ser<sup>144</sup>, Asn<sup>145</sup>, and Arg<sup>147</sup>) form a distinct cytoplasmic border from the transmembrane region. The height of these side chains is roughly comparable to that of the cytoplasmic border of C-III loop. Thus, the current model can assign a border corresponding to the major cytoplasmic part of rhodopsin. The extra membranous extension from H-VI, tentatively assigned from Thr<sup>243</sup> to Ala<sup>246</sup>, still exhibits helical structure with no obvious break. In contrast, the cytoplasmic extension of H-V breaks around Leu<sup>226</sup>, followed by an S-shaped flat loop structure almost along the surface of membrane. This connection from H-V to H-VI, the C-III loop, reaches close to the lipid-facing side of H-VI at Ala<sup>235</sup>, without covering the cytoplasmic surface of the helical bundle of rhodopsin. Thus, although our model demonstrates a highly flexible nature of this region and still lacks the tetrapeptide from Glu<sup>236</sup> to Glu<sup>239</sup>, it is obvious that C-III does not fold over the helical region at all. On the other hand, two polar side chains of Ser<sup>240</sup> and Thr<sup>242</sup> in C-III comes close to a part of COOH-terminal tail around Ser<sup>334</sup>, making a cluster of

OH groups in this region. It should be also noted that the C-III loop is known to vary considerably among related GPCRs, so the flexibility and variability of this region may be critical for functionality and specificity in G-protein activation.

The helical structure of the C-IV loop is of particular interest in the cytoplasmic region, considering previous studies of a variety of synthetic peptides and their effects on the activation of G proteins. Direct evidence for interaction of this region with the G-protein transducin has been provided using a synthetic peptide from Asn<sup>310</sup> to Leu<sup>321</sup> of bovine rhodopsin (40). The short helix is clearly distinct from H-VII and, via Met<sup>309</sup> to Lys<sup>311</sup> linker, lies nearly perpendicular to H-VII. It is also the region that follows the NPXXY motif as a part of a conserved block of residues up to Cys<sup>322</sup>. The presence of a helix for this region was demonstrated for a corresponding peptide of turkey β-adrenergic receptor by solution NMR spectroscopy in a nonpolar solvent (41). It has also been supposed that a group of peptides called mastoparans, which assume an amphiphilic helical structure and have activity on G proteins, mimic the structure of receptors in this region (42). From the rhodopsin structure, it appears that this short stretch of amino acids is located in a hydrophobic environment, which

could induce α-helical structure. The distribution of side chains along this helix also exhibits an amphiphilic pattern; the charged/polar groups cluster on one side while hydrophobic ones are on the other, suggesting that the latter, Phe<sup>313</sup>, Met<sup>317</sup> and Leu<sup>321</sup>, are buried in hydrophobic core of the receptor (Fig. 5B). Phe<sup>313</sup> and Arg<sup>314</sup> are the most conserved residues in this region, suggesting that the arrangement of this short helix in rhodopsin may be functionally important.

Although we do not include any lipid-like structure in the current model, the side chains of Cys<sup>322</sup> and Cys<sup>323</sup> project to the outside of rhodopsin, consistent with the probable attachment of palmitic acid residues (43). The helical structure appears to be terminated by Gly<sup>324</sup> and the following COOH-terminal tail changes the direction. Although current model lacks residues from 328 to 333, the positions of 327 and 334 suggest that this missing part runs covering the short H-VIII helix from the solvent region. As a whole, COOH-terminal tail of rhodopsin occupies the space over only a part of the helical bundle, H-I and H-VII. Surface potential of cytoplasmic and extracellular surfaces is shown in Web fig. 2 (22).

**Intramolecular interactions and activation.** The transmembrane region of rhodopsin is stabilized by a number of interhelical hy-

## RESEARCH ARTICLE

drogen bonds and hydrophobic interactions, and most of them are mediated by highly conserved residues in GPCRs. One of the residues that exhibit the highest conservation is Asn<sup>55</sup> in H-I. Its side chain is responsible for two interhelical hydrogen bonds to Asp<sup>83</sup> in H-II and to the peptide carbonyl of Ala<sup>299</sup> (Fig. 5C). Asp<sup>83</sup> is in turn connected via a water molecule to the peptide carbonyl of Gly<sup>120</sup> in H-III. Another region that mediates constraints for three helices includes Asn<sup>78</sup> of H-II, which is hydrogen-bonded to OH groups of Ser<sup>127</sup> of H-III and Thr<sup>160</sup>, Trp<sup>161</sup> of H-IV. Helices H-III, H-IV and H-V can be also linked through interaction among Glu<sup>122</sup>, Met<sup>163</sup>, and His<sup>211</sup>.

The tripeptide Glu<sup>134</sup>-Arg<sup>135</sup>-Tyr<sup>136</sup> is part of a highly conserved (D/E)R(Y/W) motif found in GPCRs (Fig. 5D). These residues participate in several hydrogen bonds with surrounding residues. The carboxylate of

Glu<sup>134</sup> forms salt-bridge with guanidium of the next Arg<sup>135</sup>. Arg<sup>135</sup> is also connected to Glu<sup>247</sup> and Thr<sup>251</sup> in H-VI. Val<sup>137</sup>, Val<sup>138</sup>, to Val<sup>139</sup> are also closely located to partly cover the cytoplasmic side of Glu<sup>134</sup> and Arg<sup>135</sup>. These could be one of the critical constraints keeping rhodopsin in the inactive conformation. This region has high B-values, however, and the side chains may assume different orientations.

H-VII of most of the GPCRs in the rhodopsin family contains an NPXXY sequence near the cytoplasmic end, but the functional importance of this motif remains unclear. The side chains of the two polar residues in this region, Asn<sup>302</sup> and Tyr<sup>306</sup> in bovine rhodopsin, project inside the molecule. The OH group of Tyr<sup>306</sup> is close to Asn<sup>73</sup>, which is also highly conserved among GPCRs, suggesting the presence of additional interhelical hydrogen-bonding constraints between H-VII

and H-II. Although the distance between Asn<sup>302</sup> and Asp<sup>83</sup> is too long to make a hydrogen bond, it appears possible that the water near Asp<sup>83</sup> interacts with the side chain of Asn<sup>302</sup>. In this case, this water mediates a contact among H-II, H-III, and H-VII.

The energy of light is utilized for photoisomerization of the 11-*cis*-retinal chromophore to an all-*trans*-configuration. This change in conformation would cause multiple effects, including movement of  $\beta$ -ionone toward H-III and/or displacement of Schiff base/C<sub>9</sub>/C<sub>13</sub>-methyl regions, ultimately switching the receptor to active conformation, metarhodopsin II (27, 28, 44, 45). Our model of bovine rhodopsin confirms that these effects can change the environment of the salt-bridge between the Schiff base and Glu<sup>113</sup>, resulting in its neutralization (46). Displacement of H-III will result in changing the environment of the ERY motif and its reorientation. Our rhodopsin model also

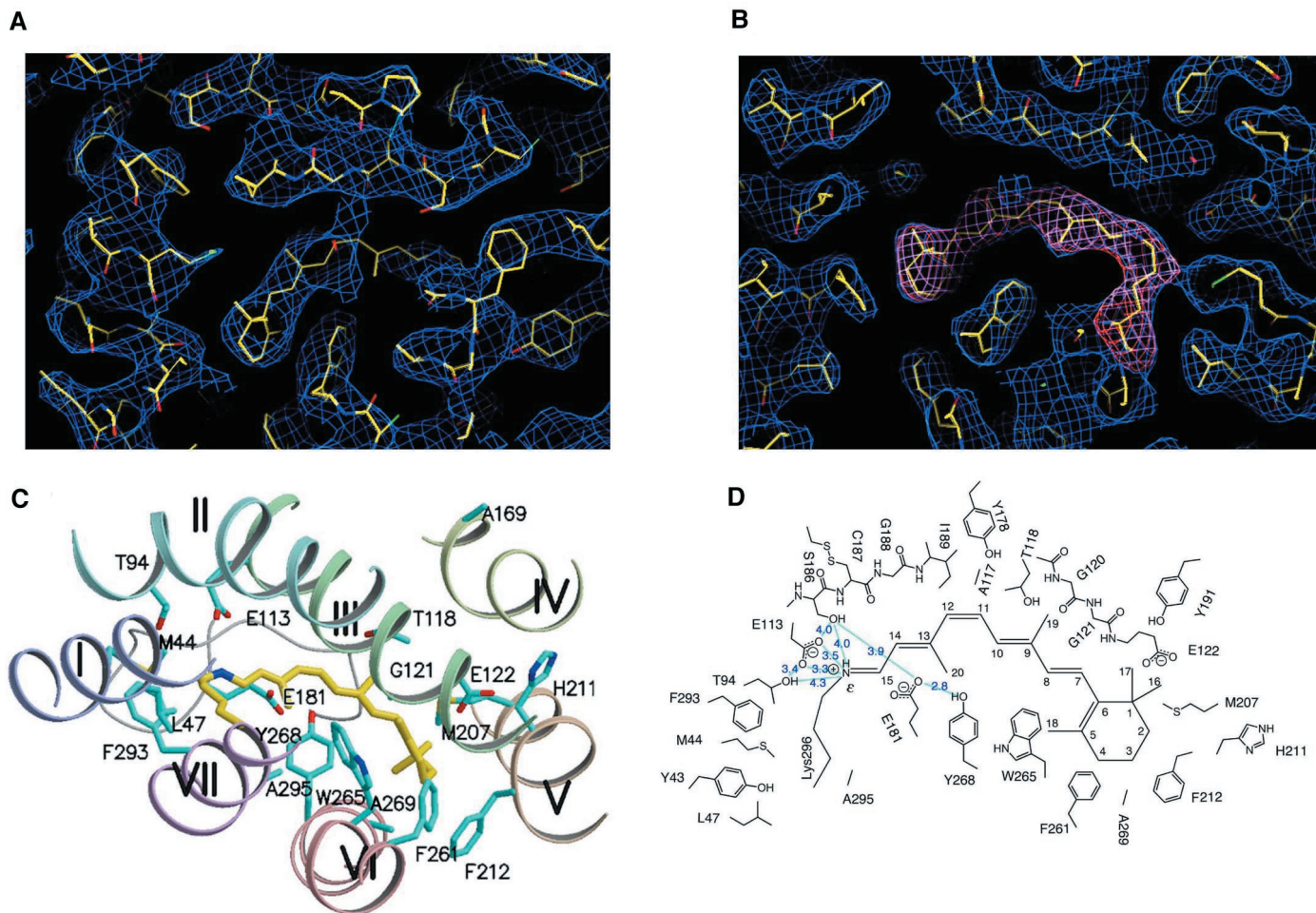


**Fig. 6.** The environment of the 11-*cis*-retinal chromophore. **(A)** Experimental electron density of 3.3 Å resolution with the final model of 3.3 Å data set using MAD phases after NCS averaging and solvent flattening with DM (20) for the retinal chromophore. Blue for  $2|F_o| - |F_c|$  map ( $1\sigma$ ). **(B)** Electron density for the retinal chromophore with the current model refined against the 2.8 Å data set. Blue for  $2|F_o| - |F_c|$  map ( $1\sigma$ ) and red for omit  $|F_o| - |F_c|$  map ( $5\sigma$ ) phases calculated using the current model. **(C)** Schematic showing the side chains

surrounding the 11-*cis*-retinylidene group, viewed from cytoplasmic side. Ala<sup>169</sup> interacts with  $\beta$ -ionone ring of all-*trans*-retinal in photoactivated states (58). When the intrinsic 11-*cis*-retinal was substituted by all-*trans*-retinal in the crystal structure, the  $\beta$ -ionone ring can reach Ala<sup>169</sup> residue. **(D)** Schematic presenting the residues within 4.5 Å distance from retinal molecule. Blue labels indicate the distances between Schiff base nitrogen atom and charged or polar atoms within 4.5 Å.

suggests that interaction between  $\beta$ -ionone ring and H-III occurs at Glu<sup>122</sup>, which is one of the residues that determine the rate of metarhodopsin II decay (47). Because Glu<sup>122</sup> interacts with His<sup>211</sup> in rhodopsin, the proposed movement of H-III caused by the  $\beta$ -ionone ring can affect the interaction between these residues in the transition to metarhodopsin II. In addition, the change around the Schiff base region can affect the interaction between the C<sub>13</sub>-methyl group of retinal and Trp<sup>265</sup>. The photoactivation may also cause breakage of some of the three interhelical constraints mediated by Ala<sup>299</sup>, Asn<sup>302</sup>, and Tyr<sup>306</sup>, and hydrophobic constraints via Phe<sup>294</sup> to the highly kinked region in H-VI. As a result, rearrangement of the helical bundle may be triggered, and finally lead to the movements of H-III and/or H-VI (48). Our proposed mechanism stresses importance of the chromophore in the activation process, in agreement with the physiology of photoreceptor cells. Ideally, for a complete picture of the activation process, high-resolution structures of intermediates of photolyzed rhodopsin will be necessary.

**Summary.** The GPCR family is one of the largest and most diverse groups of proteins encoded by 1 to 3% of the genes present in our genome. They are involved in many physiological processes and are attractive targets for pharmacological intervention to modify these processes in normal and pathological states. The crystal structure of rhodopsin reveals a highly organized heptahelical transmembrane bundle with 11-*cis*-retinal as a key cofactor involved in maintaining rhodopsin in the ground state. A set of residues that interacts with the 11-*cis*-retinal chromophore produces the environment that results in an absorption shift of the chromophore to a longer wavelength. The structure provides insight into the spectral tuning of related receptors, cone pigments. The structure also gives information on the molecular mechanism of GPCR activation. A conserved set of residues on the cytoplasmic surface, where G-protein activation occurs, likely undergo a conformational change upon photoactivation of the chromophore that leads to rhodopsin activation and signal transduction.

#### References and Notes

- P. A. Hargrave and J. H. McDowell, *FASEB J.* **6**, 2323 (1992).
- T. P. Sakmar, *Prog. Nucleic Acid Res. Mol. Biol.* **59**, 1 (1998).
- Y. Shichida and H. Imai, *Cell. Mol. Life Sci.* **54**, 1299 (1998).
- G.T. Iiri, Z. Farfel, H. R. Bourne, *Nature* **394**, 35 (1998).
- T. P. Dryja et al., *Nature* **343**, 364 (1990).
- Y. A. Ovchinnikov, *FEBS Lett.* **148**, 179 (1982).
- P. A. Hargrave et al., *Biophys. Struct. Mech.* **9**, 235 (1983).
- T. Yoshizawa and G. Wald, *Nature* **197**, 1279 (1963).
- B. K.-K. Fung and L. Stryer, *Proc. Natl. Acad. Sci. U.S.A.* **77**, 2500 (1980).
- S. Hecht, S. Shlaer, M. H. Pirenne, *J. Gen. Physiol.* **25**, 819 (1942).
- V. M. Unger, P. A. Hargrave, J. M. Baldwin, G. F. X. Schertler, *Nature* **389**, 203 (1997).
- J. M. Baldwin, *EMBO J.* **12**, 1693 (1993).
- T. Shieh, M. Han, T. P. Sakmar, S. O. Smith, *J. Mol. Biol.* **269**, 373 (1997).
- I. D. Pogozhva, A. L. Lomize, H. I. Mosberg, *Biophys. J.* **72**, 1963 (1997).
- P. Herzyk and R. E. Hubbard, *J. Mol. Biol.* **281**, 741 (1998).
- Z. T. Farahbakhsh, K. D. Ridge, H. G. Khorana, W. L. Hubbell, *Biochemistry* **34**, 8812 (1995).
- J.-M. Kim, C. Altenbach, R. L. Thurmond, H. G. Khorana, W. L. Hubbell, *Proc. Natl. Acad. Sci. U.S.A.* **94**, 14273 (1997).
- O. P. Ernst et al., *J. Biol. Chem.* **275**, 1937 (2000).
- T. Okada et al., *J. Struct. Biol.* **130**, 73 (2000).
- The tetragonal crystals of rhodopsin have been obtained by using purified protein from bovine rod outer segment (ROS) membranes (19, 49), and derivatized by soaking for about 2 months in a few mM solution of mercury acetate. To avoid deterioration of crystals by visible light, all of the experimental procedures involving rhodopsin were carried out under dim red light. The unit cell dimensions are  $a = b = \sim 96.5 \text{ \AA}$ , and  $c = 149.5 \text{ \AA}$ , with larger deviations up to 1.5  $\text{\AA}$  in the  $a$  and  $b$  dimensions. The previous assignment of the space group as P4<sub>1</sub>22 or P4<sub>3</sub>22 (19) for native crystal is incorrect. Instead, the crystals are merohedrally twinned, with space group P4<sub>1</sub>, with two rhodopsin molecules in the asymmetric unit. Table 1 contains information about the crystal, the tetragonal heavy atom derivative, the MAD phasing, and the structure refinement. The least twinned data set was selected after the collection of several MAD data sets. Six-wavelength MAD data sets were collected using only one crystal with a twin ratio of 10% at SPring-8 BL45XU (50) on a R-AXIS IV, after measurement of the XANES spectrum of another mercury derivative for the determination of the Hg absorption edge wavelength. The intensity data were integrated and scaled with DENZO and SCALEPACK (51). Twinning ratio of the data was estimated with CNS (52), but the data were processed as collected, without any consideration for twinning. Crystallographic calculation was performed including the model-refinement using this 3.3  $\text{\AA}$  MAD data set. SOLVE (53) performed local scaling and found four mercury sites in the asymmetric unit, and phase refinement was successively done by SHARP (54). The MAD phased electron density map could be traced and fit with 14  $\alpha$  helices from two monomers. The noncrystallographic symmetry (NCS) operator and molecular masks were obtained from the helices. Density modifications including NCS averaging were performed with DM/CCP4 (55). Most of the protein region including side chains could be recognized except loops C-II and C-III and the COOH-terminal portion in the map. The oligosaccharide chains from Asn<sup>2</sup> and Asn<sup>15</sup> were also partially found. Iterative simulated annealing and rebuilding of the model were carried out with CNS (52) and O (56). The  $R$ -value and free  $R$  were 23.9% and 28% for the 3.3  $\text{\AA}$  data at the final stage. The higher resolution model refinement has proceeded using a 2.8  $\text{\AA}$  data set collected at APS 19-ID, using the 3.3  $\text{\AA}$  structure as the starting model and its MAD phased data with the experimental phase restraint option of CNS. The 2.8  $\text{\AA}$  data set was collected from a mercury-soaked crystal. The estimation of the twin fraction and detwining of the data were performed with CNS. The model structure was validated using PROCHECK (57).
- M. N. Fukuda, D. S. Papermaster, P. A. Hargrave, *J. Biol. Chem.* **254**, 8201 (1979).
- Web figures 1 and 2 are available at [www.sciencemag.org/feature/data/1053064.shl](http://www.sciencemag.org/feature/data/1053064.shl)
- H. Luecke, B. Schober, H.-T. Richter, J.-P. Cartailler, J. K. Lanyi, *J. Mol. Biol.* **291**, 899 (1999).
- H. Belrhali et al., *Struct. Folding Des.* **7**, 909 (1999).
- M. Kolbe, H. Besir, L.-O. Essen, D. Oesterhelt, *Science* **288**, 1390 (2000).
- V. R. Rao, G. B. Cohen, D. D. Oprian, *Nature* **367**, 639 (1994).
- T. P. Sakmar, R. R. Franke, H. G. Khorana, *Proc. Natl. Acad. Sci. U.S.A.* **86**, 8309 (1989).
- E. A. Zhukovsky and D. D. Oprian, *Science* **246**, 928 (1989).
- Single-letter abbreviations for the amino acid residues are as follows: A, Ala; C, Cys; D, Asp; E, Glu; F, Phe; G, Gly; H, His; I, Ile; K, Lys; L, Leu; M, Met; N, Asn; P, Pro; Q, Gln; R, Arg; S, Ser; T, Thr; V, Val; W, Trp; and Y, Tyr. X indicates any residue.
- R. H. Callender, A. Doukas, R. Crouch, K. Nakanishi, *Biochemistry* **15**, 1621 (1976).
- I. Palings et al., *Biochemistry* **26**, 2544 (1987).
- S. O. Smith et al., *Biochemistry* **26**, 1606 (1987).
- P. K. Brown and G. Wald, *J. Biol. Chem.* **222**, 865 (1956).
- D. D. Thomas and L. Stryer, *J. Mol. Biol.* **154**, 145 (1982).
- T. Ebrej, M. Tsuda, G. Sassenrath, J. L. West, W. H. Waddell, *FEBS Lett.* **116**, 217 (1980).
- M. Neitz, J. Neitz, G. H. Jacobs, *Science* **252**, 971 (1991).
- Z. Wang, A. B. Asenjo, D. D. Oprian, *Biochemistry* **32**, 2125 (1993).
- T. Doi, R. S. Molday, H. G. Khorana, *Proc. Natl. Acad. Sci. U.S.A.* **87**, 4991 (1990).
- A. F. L. Creemers et al., *Biochemistry* **38**, 7195 (1999).
- B. Konig et al., *Proc. Natl. Acad. Sci. U.S.A.* **86**, 6878 (1989).
- H. Jung, R. Windhaber, D. Palm, K. D. Schnackerz, *Biochemistry* **35**, 6399 (1996).
- K. Wakamatsu, A. Okada, T. Miyazawa, M. Ohya, T. Higashijima, *Biochemistry* **31**, 5654 (1992).
- Y. A. Ovchinnikov, N. G. Abdulaev, A. S. Bogachuk, *FEBS Lett.* **230**, 1 (1988).
- R. G. Matthews, R. Hubbard, P. K. Brown, G. Wald, *J. Gen. Physiol.* **47**, 215 (1963).
- C. K. Meyer et al., *J. Biol. Chem.* **275**, 19713 (2000).
- P. R. Robinson, G. B. Cohen, E. A. Zhukovsky, D. D. Oprian, *Neuron* **9**, 719 (1992).
- H. Imai et al., *Proc. Natl. Acad. Sci. U.S.A.* **94**, 2322 (1997).
- D. L. Farrens, C. Altenbach, K. Yang, W. L. Hubbell, H. G. Khorana, *Science* **274**, 768 (1996).
- T. Okada, K. Takeda, T. Kouyama, *Photochem. Photobiol.* **65**, 495 (1998).
- M. Yamamoto, T. Kumasaka, T. Fujisawa, T. Ueki, *J. Synchrotron Radiat.* **5**, 222 (1998).
- Z. Otwinowski and W. Minor, *Methods Enzymol.* **276**, 307 (1997).
- A. T. Brünger et al., *Acta Crystallogr. D* **54**, 905 (1998).
- T. C. Terwilliger and J. Berendzen, *Acta Crystallogr. D* **55**, 849 (1999).
- E. de La Fortelle and G. Bricogne, *Methods Enzymol.* **276**, 472 (1997).
- K. Cowtan, *Joint CCP4 and ESF-EACBM Newsletter on Protein Crystallography* **31**, 34 (1994).
- T. A. Jones, S. Cowan, J. Y. Zou, M. Kjeldgaard, *Acta Crystallogr. A* **47**, 110 (1991).
- R. A. Laskowski, M. W. MacArthur, D. S. Moss, J. M. Thornton, *J. Appl. Crystallogr.* **26**, 283 (1993).
- B. Borhan, M. L. Souto, H. Imai, Y. Shichida, K. Nakanishi, *Science* **288**, 2209 (2000).
- We are grateful to P. Van Hooser for sample preparation and support for this project; E. Merritt, S. Turley, M. Feese, and S. Suresh for their help in the experiment at APS; and Y. Imamoto for the template artwork for Fig. 3. We thank the Stanford Synchrotron Radiation Laboratory for beam time for the initial stages of this study. Use of the Argonne National Laboratory Structural Biology Center beamlines at the Advanced Photon Source (APS) was supported by the U.S. Department of Energy, Office of Biological and Environmental Research under contract W-31-109-ENG-38. Coordinates for bovine rhodopsin have been deposited in the Protein Data Bank (1F88). This research was supported by NIH grant EY09339, a grant from Research to Prevent Blindness, Inc. (RPB Foundation) to the Department of Ophthalmology at the University of Washington, and grants from Foundation Fighting Blindness, Inc., the Ruth and Milton Steinbach Fund, and the E. K. Bishop Foundation. This paper is dedicated to T. Yoshizawa.

12 June 2000; accepted 5 July 2000